Supporting Information

Controlled formation of multi-scale porosity in ionosilica templated by ionic liquid

Shilpa Sharma,[1] Julian Oberdisse,[2*] Johan G. Alauzun,[1] Philippe Dieudonné-George,[2] Thomas Bizien,[3] Cansu Akkaya,[2] Peter Hesemann,[1] Anne-Caroline Genix[2*]

[1]*ICGM, Université de Montpellier, CNRS, ENSCM, 34095 Montpellier, France*

[2]*Laboratoire Charles Coulomb (L2C), Université de Montpellier, CNRS, F-34095 Montpellier, France*

[3]*SOLEIL Synchrotron, L'Orme des Merisiers, Gif-Sur-Yvette, 91192 Saint-Aubin, France*

* Corresponding authors: anne-caroline.genix@umontpellier.fr; julian.oberdisse@umontpellier.fr

1. Samples

The detailed list of the 25 samples studied in this work is given in Tables S1 and S2 for films and monoliths, respectively.

Table S1. Composition of the ionosilica films. n_{TTA} and v_{TTA}, number of moles and volume of tris(3-(trimethoxysilyl)propyl)amine (TTA); n_{IL} and v_{IL}, number of moles and volume of 1-butyl-3-methylimidazolium bis(trifluoromethylsulfonyl)imide (IL = BMIM-TFSI); $v_{Ethanol}$ volume of ethanol; v_{HCl} volume of the HCl solution at 0.6 M; Φ_{IS} volume fraction of ionosilica; Φ_{IL} = 100 - Φ_{IS} volume fraction of ionic liquid; Φ_{meso} volume fraction of mesopores; Φ_{macro} volume fraction of macropores (Φ_{meso} + Φ_{macro} = Φ_{IL}).

FILMS	TTA precursor		Ionic liquid		Ethanol	HCl solution	Φ_{IS} (%v)	Φ_{IL} (%v)	Φ_{meso} (%v)	Φ_{macro} (%v)
	n_{TTA} (mmol)	v_{TTA} (ml)	n_{IL} (mmol)	v_{IL} (mL)	$v_{Ethanol}$ (mL)	v_{HCl} (mL)				
1	6.5	3.0	3.4	1.0	3.0	0.65	48.6	51.4	38.1	13.3
2	6.5	3.0	10.2	3.0	3.0	0.65	21.5	78.5	29.8	48.7
3	6.5	3.0	10.2	3.0	3.0	0.65	26.6	73.4	42.3	31.2
4	6.5	3.0	10.2	3.0	3.0	0.65	31.0	69.0	21.3	47.7
5	6.5	3.0	20.5	6.0	3.0	0.65	16.3	83.7	14.0	69.7
6	6.5	3.0	20.5	6.0	3.0	0.65	13.7	86.3	8.4	77.9
7	6.5	3.0	20.5	6.0	3.0	0.65	15.2	84.8	18.4	66.4
8	6.5	3.0	20.5	6.0	3.0	0.65	14.3	85.7	16.0	69.6
9	6.5	3.0	20.5	6.0	3.0	0.65	15.9	84.1	8.4	75.8
10	6.5	3.0	40.9	12.0	3.0	0.65	4.2	95.8	6.7	89.1
11	6.5	3.0	40.9	12.0	3.0	0.65	5.6	94.4	11.8	82.6

Table S2. Composition of the ionosilica monoliths. n_{TTA} and v_{TTA}, number of moles and volume of tris(3-(trimethoxysilyl)propyl)amine (TTA); n_{IL} and v_{IL}, number of moles and volume of 1-butyl-3-methylimidazolium bis(trifluoromethylsulfonyl)imide (IL = BMIM-TFSI); v_{HCOOH} volume of formic acid; Φ_{IS} volume fraction of ionosilica; Φ_{IL} = 100 - Φ_{IS} volume fraction of ionic liquid; Φ_{meso} volume fraction of mesopores; Φ_{macro} volume fraction of macropores (Φ_{meso} + Φ_{macro} = Φ_{IL}).

MONOLITHS	TTA precursor		Ionic liquid		Formic acid	Φ_{IS} (%v)	Φ_{IL} (%v)	Φ_{meso} (%v)	Φ_{macro} (%v)
	n_{TTA} (mmol)	v_{TTA} (ml)	n_{IL} (mmol)	v_{IL} (mL)	v_{HCOOH} (mL)				
1	6.5	3.0	3.4	1.0	2	84.2	15.8	0	15.8
2	6.5	3.0	3.4	1.0	2	90.3	9.7	0	9.7
3	6.5	3.0	3.4	1.0	2	87.0	13.0	0	13.0
4	6.5	3.0	10.2	3.0	2	72.4	27.6	1.8	25.8
5	6.5	3.0	10.2	3.0	2	67.0	33.0	0	33.0
6	6.5	3.0	10.2	3.0	2	61.8	38.2	8.4	29.8
7	6.5	3.0	20.5	6.0	2	54.9	45.1	25.8	19.3
8	6.5	3.0	20.5	6.0	2	62.2	37.8	26.3	11.5
9	6.5	3.0	20.5	6.0	2	20.3	79.7	12.3	67.5
10	6.5	3.0	20.5	6.0	2	27.3	72.7	17.5	55.2
11	6.5	3.0	20.5	6.0	2	49.8	50.2	25.5	24.7
12	6.5	3.0	40.9	12.0	2	19.2	80.8	10.6	70.3
13	6.5	3.0	40.9	12.0	2	25.6	74.4	19.7	54.7
14	6.5	3.0	40.9	12.0	2	20.5	79.5	15.0	64.6

2. Thermogravimetric analysis (TGA)

Figure S1 shows the thermograms of the pure ionic liquid and a set of different composites – films and monoliths – containing various amount of IL. The higher the nominal amount of IL, the lower the residual mass, with the shape of the thermogram approaching that of the pure ionic liquid. The thermogram of the pure ionosilica scaffold obtained after washing is also given in both cases.

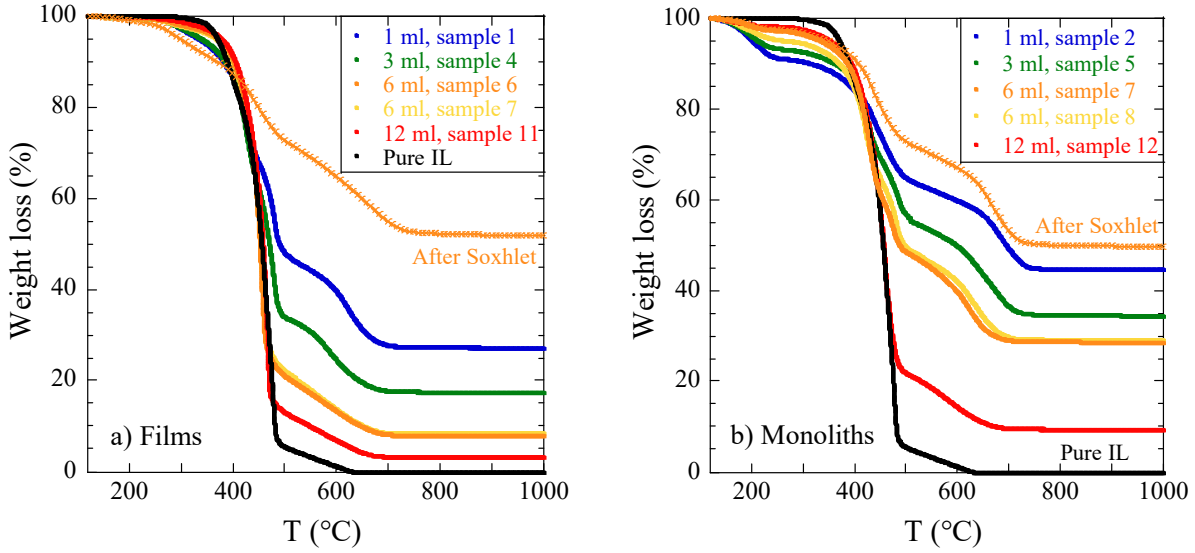

Figure S1. TGA curves normalized to the weight loss at 120°C of films (a) and monoliths (b). The pure IL is given in black. Crosses stand for the 6 ml composites (orange circles) after Soxhlet to remove the ionic liquid. Sample numbers refer to Tables S1 and S2 for films and monoliths, respectively.

3. Determination of the wash time for IL extraction

To test the efficiency of IL extraction, a series of monoliths and films (v_{IL} = 6 ml) were measured after different wash times by TGA and SAXS, which is highly sensitive to the presence of ionic liquid in the high-q range. The corresponding data are shown in Figures S2 and S3 for the films and monoliths, respectively. In Figures S2a and S3a, the total weight loss levels off after one night, but only after two days there is a superposition of the data with a broadened degradation of the organic ionosilica part between ca. 300 and 450°C. In parallel, one can see by SAXS the increased visibility of the mesoporous structure as the pores are emptied. Here also, the high-q data for the 2-day and 5-day wash times are superimposed on each other in the range of the atomic correlations.

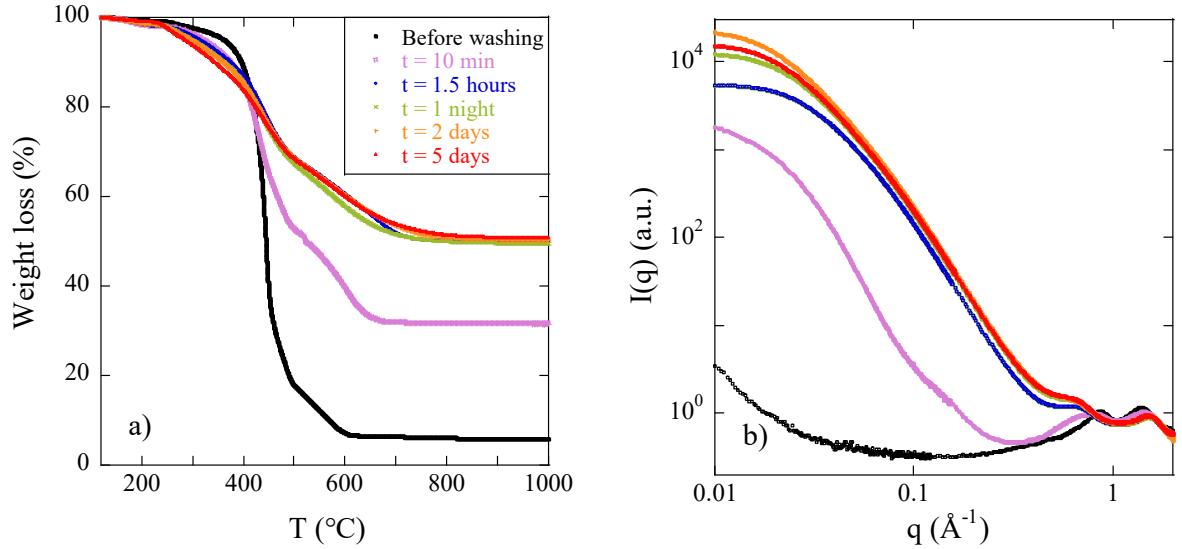

Figure S2. (a) TGA curves normalized to the weight loss at 120°C of a series of films with v_{IL} = 6 ml after different wash times. Black dots represent the original IS/IL sample before washing. The shortest wash is performed by dipping the sample in a beaker of ethanol. The following washes are performed in Soxhlet (each cycle takes approximately 30 minutes). (b) SAXS intensity of the same samples normalized at high q for comparison.

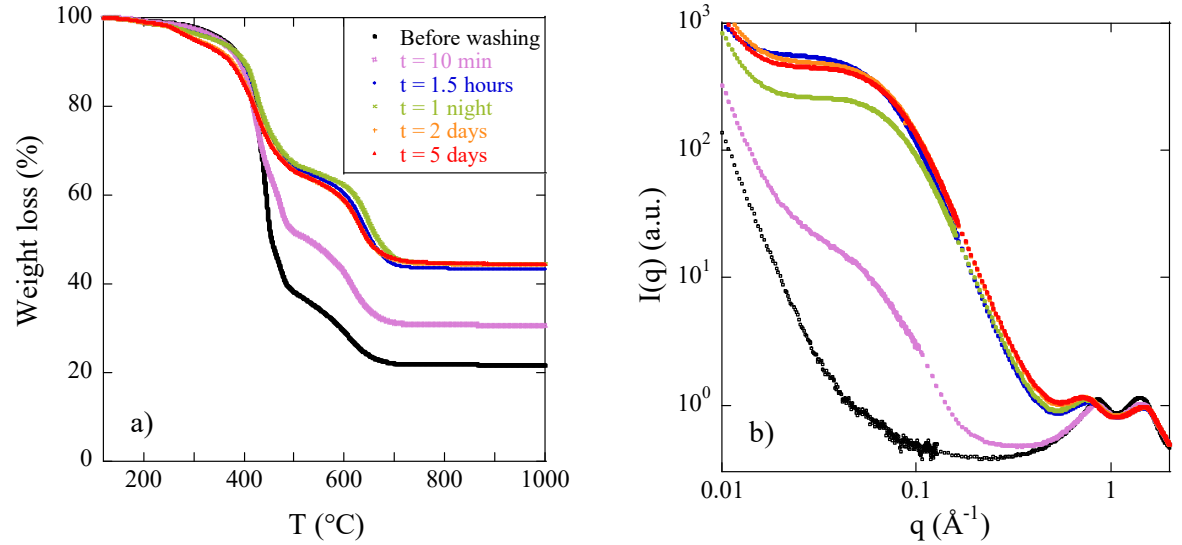

Figure S3. (a) TGA curves normalized to the weight loss at 120°C of a series of monoliths with v_{IL} = 6 ml after different wash times. Black dots represent the original IS/IL sample before washing. The shortest wash is performed by dipping the sample in a beaker of ethanol. The following washes are performed in Soxhlet (each cycle takes approximately 30 minutes). (b) SAXS intensity of the same samples normalized at high q for comparison.

4. Fraction of incorporated IL

The efficiency of IL incorporation is shown in Figure S4 in terms of successfully incorporated IL in IS. This quantity is expressed as the ratio of the IL volume fraction effectively incorporated (from TGA) to the nominal one, Φ_{IL}(TGA)/Φ_{IL}(nominal).

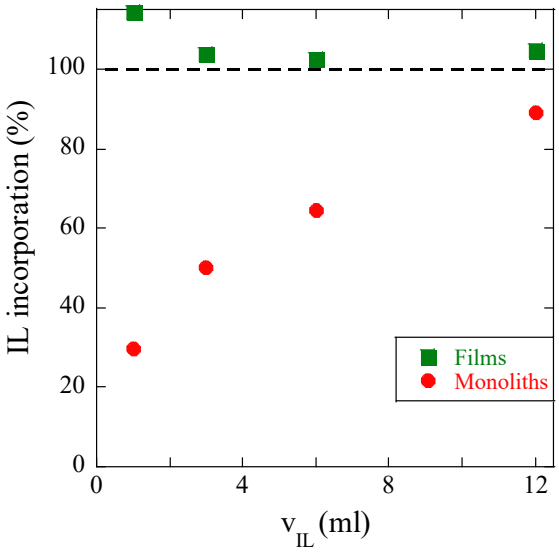

Figure S4. Retained volume fraction of the ionic liquid in the ionosilica matrix for films (squares) and monoliths (circles) as a function of the nominal amount of ionic liquid introduced. This fraction corresponds to the ratio Φ_{IL}(TGA)/Φ_{IL}(nominal).

5. Complementary BET results

Analysis of the specific surface: The BET equation is applied in the linear form for relative pressures p/p_0 between 0.05 and 0.35 in Figure S5. The BET parameters v_m and C can be deduced from the slope A and y-intercept B: $v_m = 1/(A+B)$ and $C = 1 + A/B$.

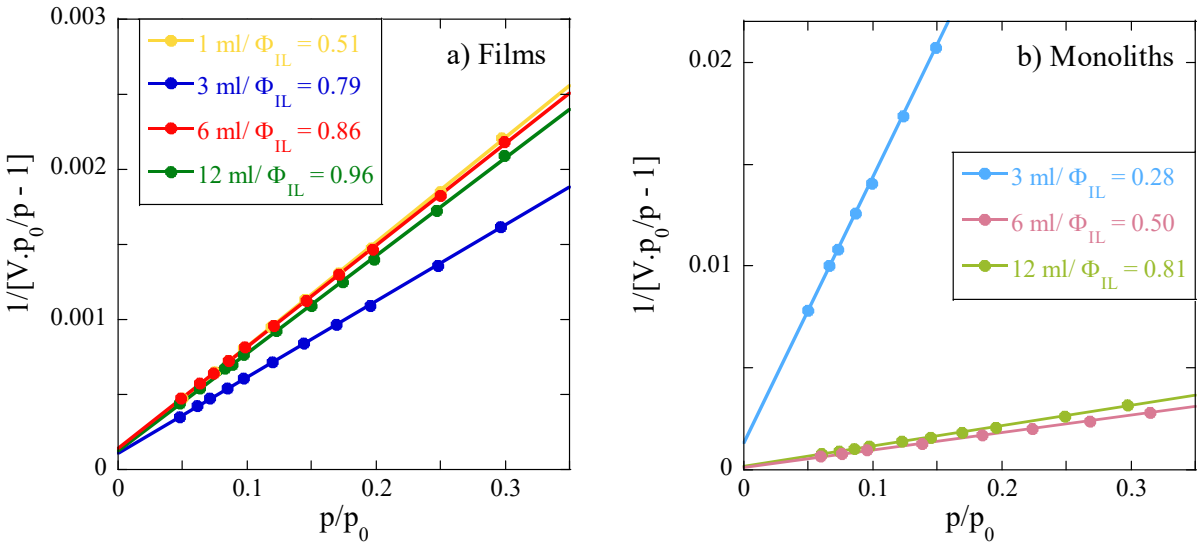

Figure S5. $[V\ (p_0/p-1)]^{-1}$ as a function of relative pressure for films (a) and monoliths (b). V is the adsorbed quantity in cm^3/g.

Pore size distributions: The distributions in volume are shown in Figure S6 for the mesoporous samples described in Tables S1 and S2. They are obtained by taking the incremental pore volume in cm^3/g during adsorption and multiplying by βd, where d is the density of the sample after washing ($d = d_{IS}\Phi_{IS}$). The area under each curve in Figure S6 is equal to $\beta\Phi_{meso}$ (see eq.(8)).

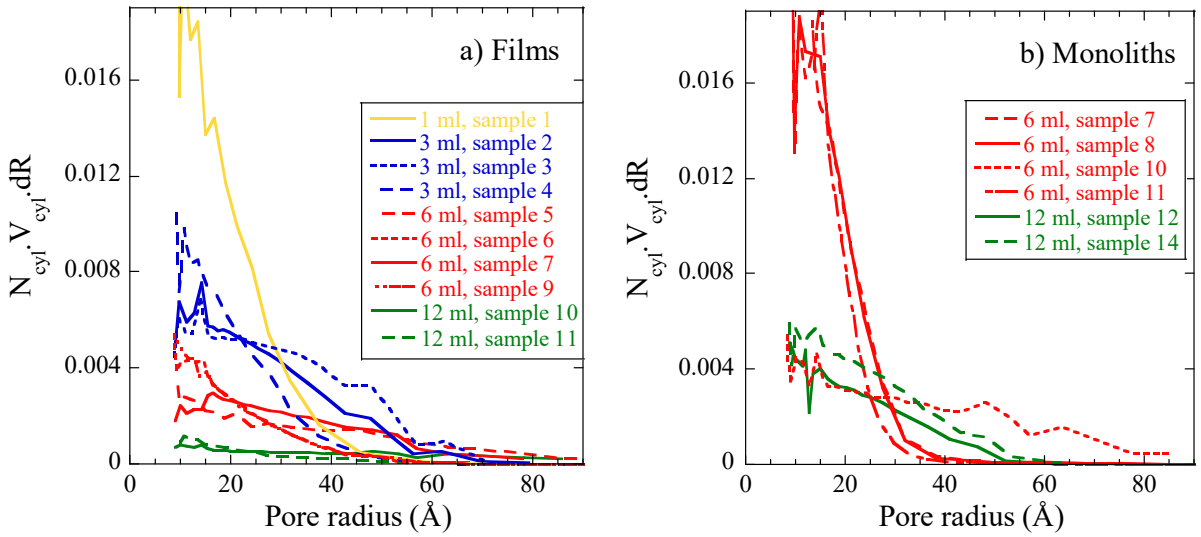

Figure S6. Pore size distribution of cylinders calculated using eq.(9) from BJH data expressed as contribution to the total volume fraction for films (a) and monoliths (b).

Volume fraction of mesopores: The total volume fraction of mesopores Φ_{meso} as seen by adsorption is plotted in Figure S7 together with Φ_{macro} and $\Phi_{IS} = 1 - \Phi_{IL}$ as a function of the final pore volume fraction given by Φ_{IL} ($\Phi_{IL} = \Phi_{meso} + \Phi_{macro}$).

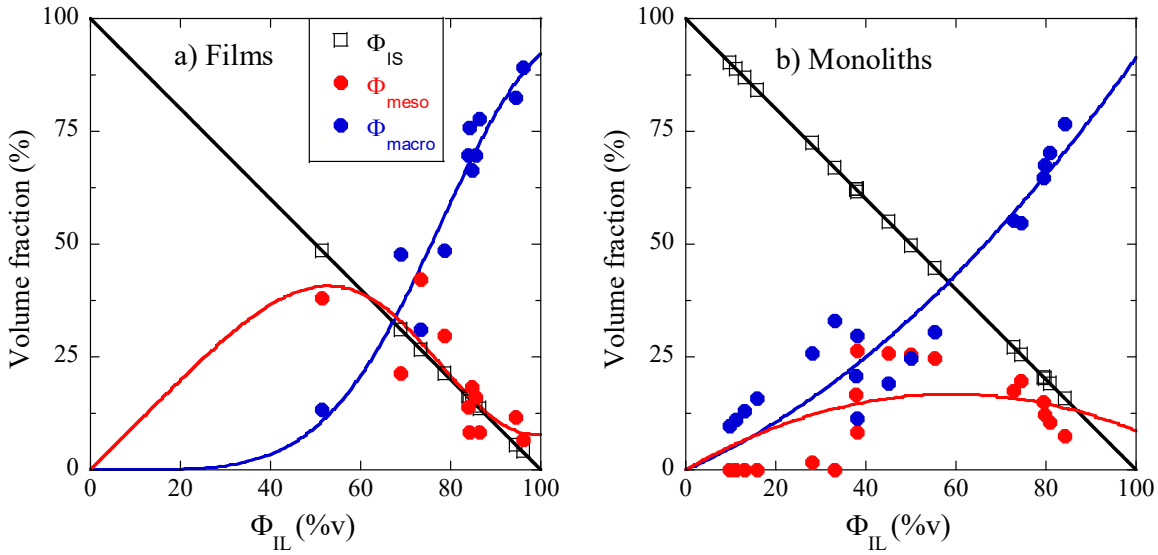

Figure S7. Volume fractions of ionosilica and mesopores in (a) films and (b) monoliths as a function of Φ_{IL}. The remaining volume fraction Φ_{macro} corresponds to pores which are too big to be captured by BET. Lines are guides to the eye respecting the conservation of volume given by eq. (3b).

6. Complementary TEM results

TEM pictures of films and monoliths prepared with 6 ml of ionic liquid are shown in Figure S8 after washing.

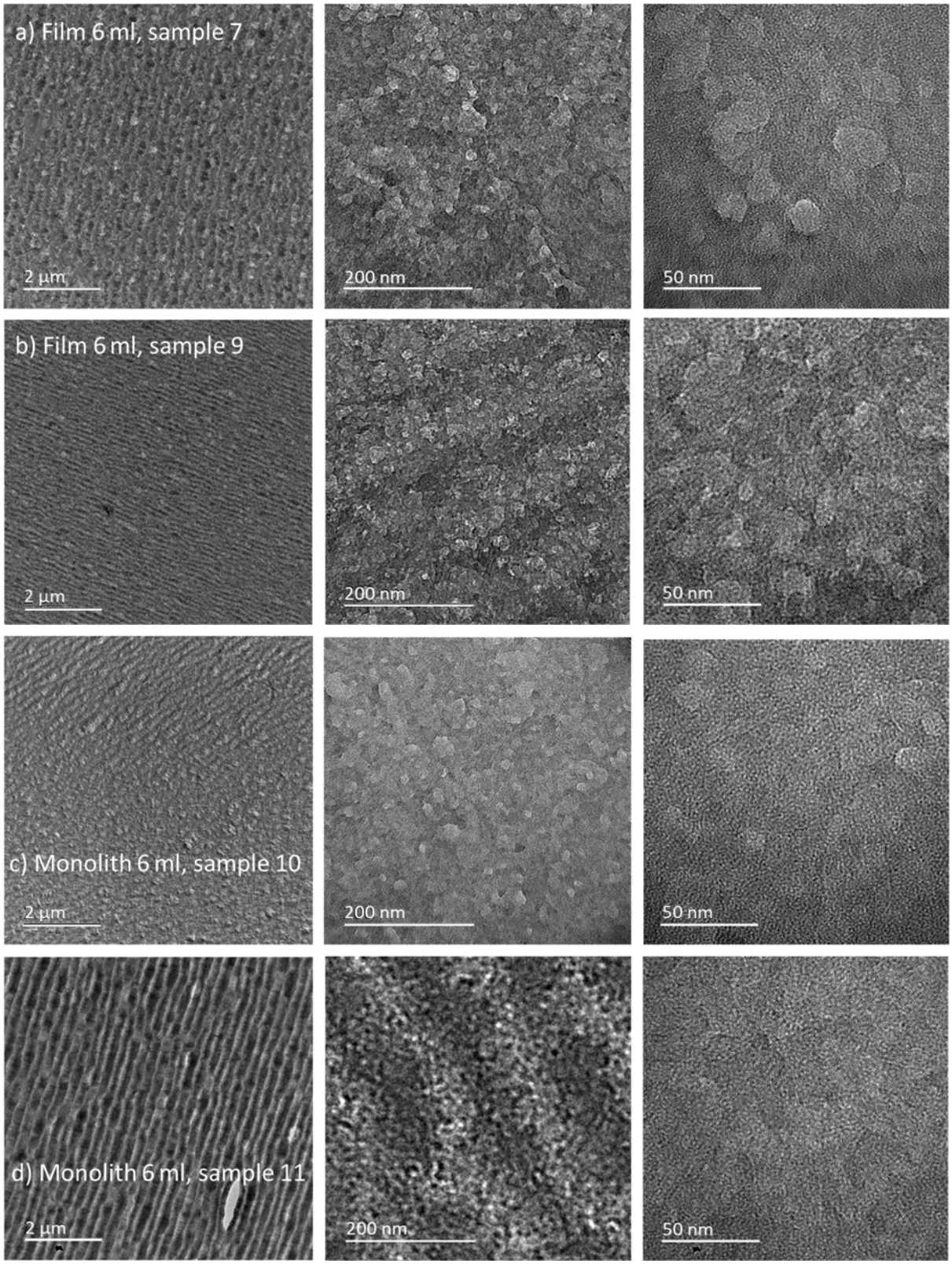

Figure S8. High-resolution TEM pictures of ionosilica composites after Soxhlet washing for three magnifications. (a) and (b) Films, and (c) and (d) monoliths. v_{IL} = 6 ml in the four cases, see Table S1 and S2 for sample details.

7. Complementary SAXS results

The SAXS data given in Figure 6 have been normalized by Φ_{IS}. The same data without normalization and normalized by Φ_{meso} are shown in Figures S9 and S10 for films and monoliths, respectively. Higher normalized I_0/Φ_{meso} intensities go with higher average pore volume, which is found to follow the IL content. The superposition in the mid-q range can be interpreted as coming from a similar local scale generating the specific surface, i.e., lateral pore dimension varying within a factor of two (Figure 8).

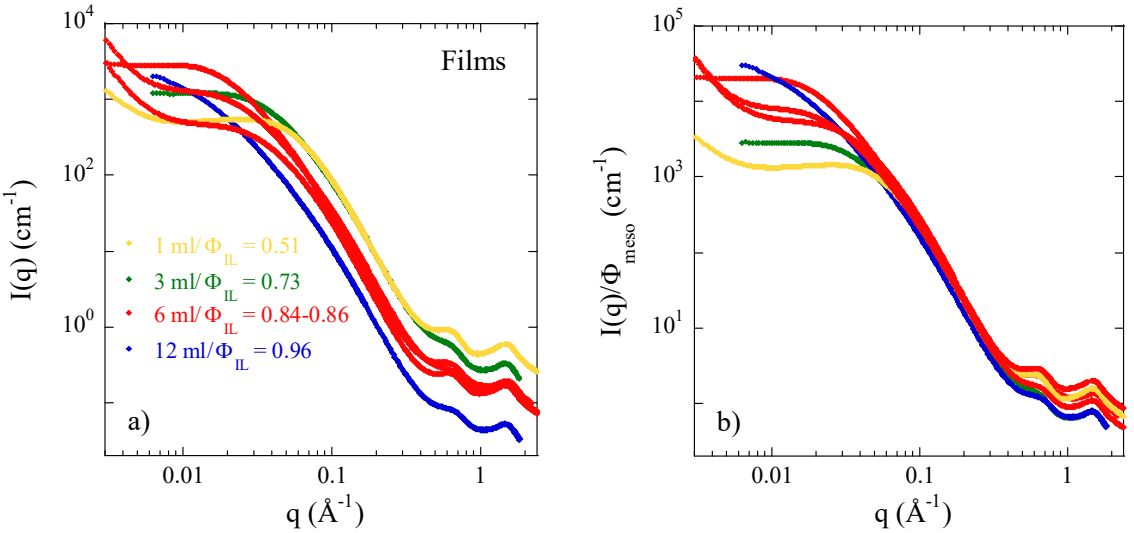

Figure S9. Scattered intensities for different IL-contents of emptied films without normalization (a) and normalized by Φ_{meso} (b). The color code gives the quantity of templating-IL introduced as indicated by the legend. The corresponding IL volume fraction is also indicated.

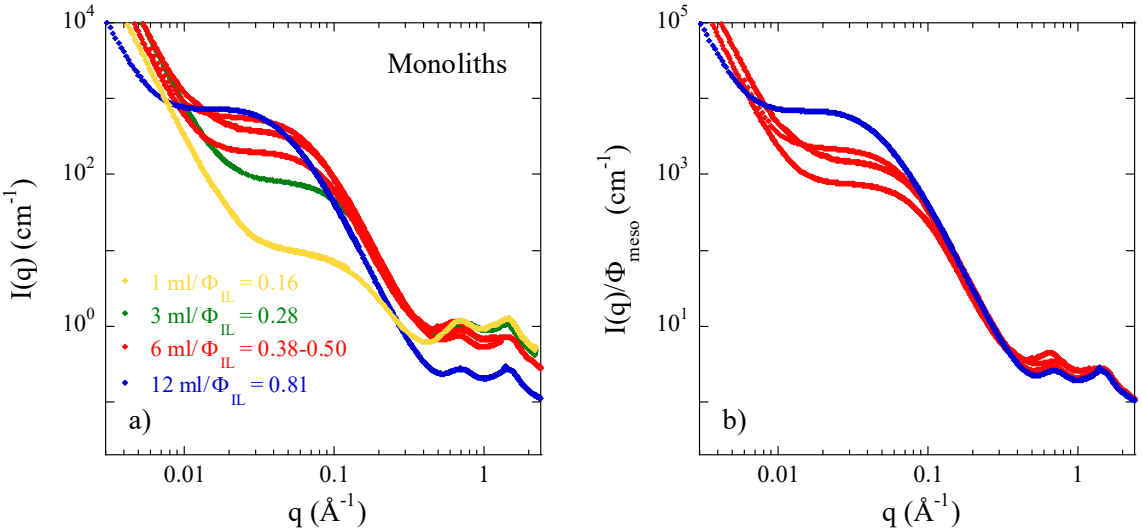

Figure S10. Scattered intensities for different IL-contents of emptied monoliths without normalization (a) and normalized by Φ_{meso} (b). The color code gives the quantity of templating-IL introduced as indicated by the legend. The corresponding IL volume fraction is also indicated. There are no data in b) for v_{IL} = 1 and 3 ml since no mesoporosity has been detected by BET in the corresponding samples.

Different descriptions of the mesoporosity are shown in Figure S11, using polydisperse spheres or cylinders. The fitted intensity in Figure S11 coincides with the measured intensity within a factor 0.69 for spheres with a Gaussian distribution in size, 1.17 for cylinders with Gaussian distribution and 1.54 for cylinders with BJH distribution. The best shape description is given by BJH and the worst by spheres.

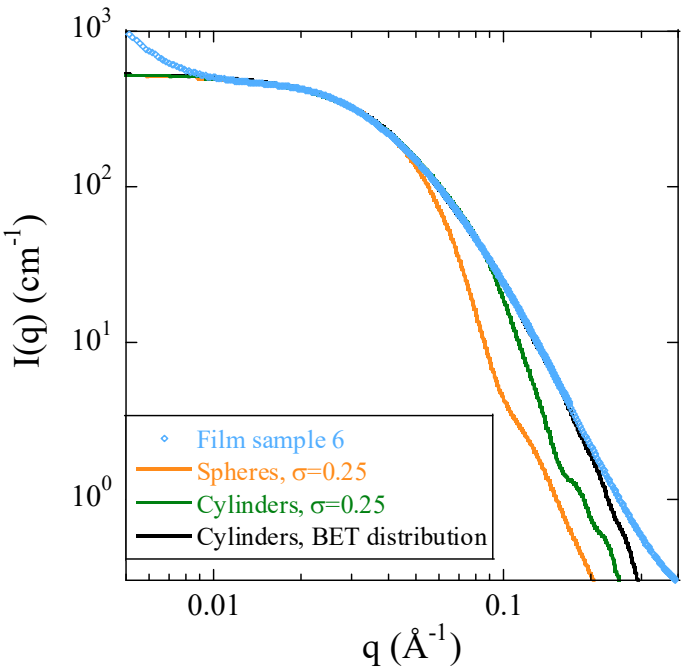

Figure S11. Example of fits (solid lines) of an emptied film sample (v_{IL} = 6 ml, sample 6 in Table S1, blue symbols) by polydisperse spheres ($<R_s>$ = 3.9 nm, orange) and radially polydisperse cylinders (L_{cyl} = 12.8 nm, $<R_{cyl}>$ = 2.3 nm, green) both using a Gaussian distribution with σ = 25%. The best fit is obtained by considering polydisperse cylinders with the radius distribution function deduced from BJH (L_{cyl} = 11 nm, $<R_{cyl}>$ = 1.7 nm, black). In the latter case, β = 1 (spheres are not needed).

Figures S12 and S13 show exemplary fits of the SAXS data of some films and monoliths after IL extraction. In some rare cases, a maximum in intensity is observed (e.g., Figure S12a), which is presumably related to some higher ordering of the pores.

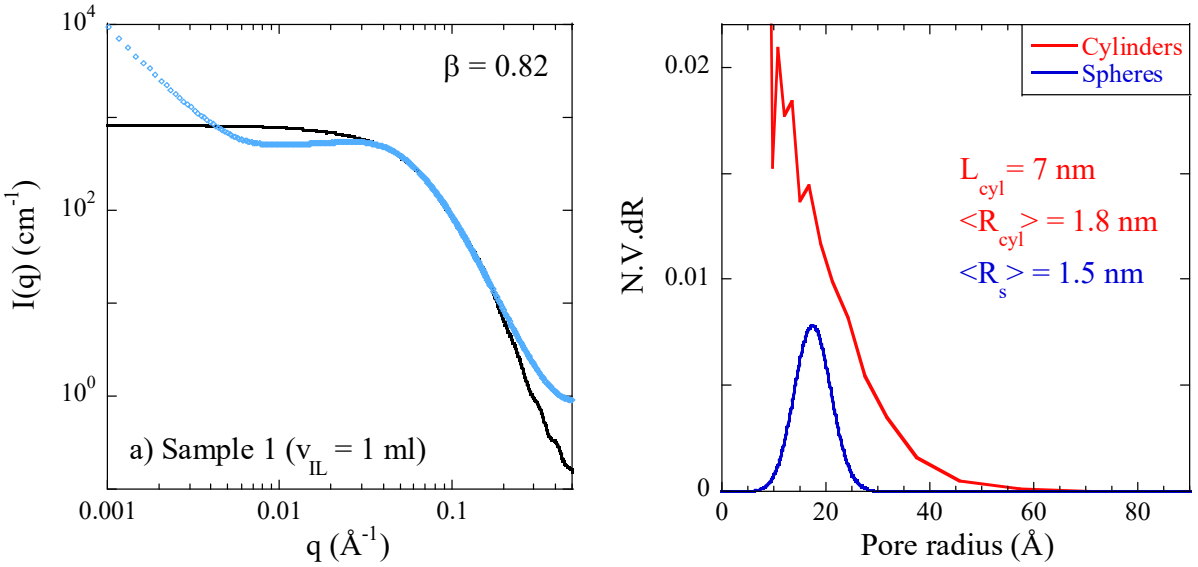

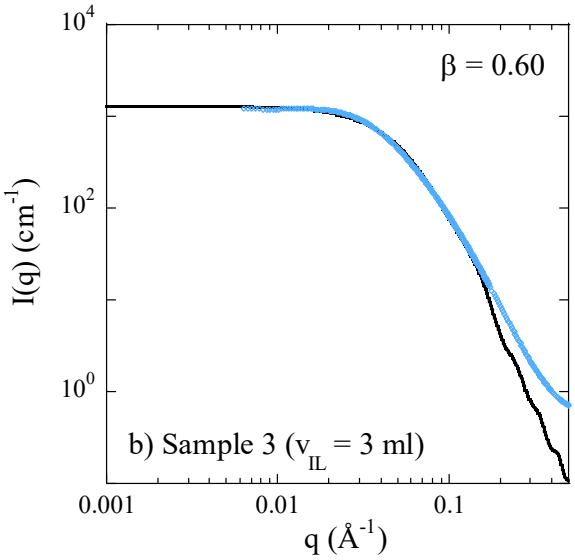
β = 0.60
b) Sample 3 (v_IL = 3 ml)
I(q) (cm^-1)
q (Å^-1)

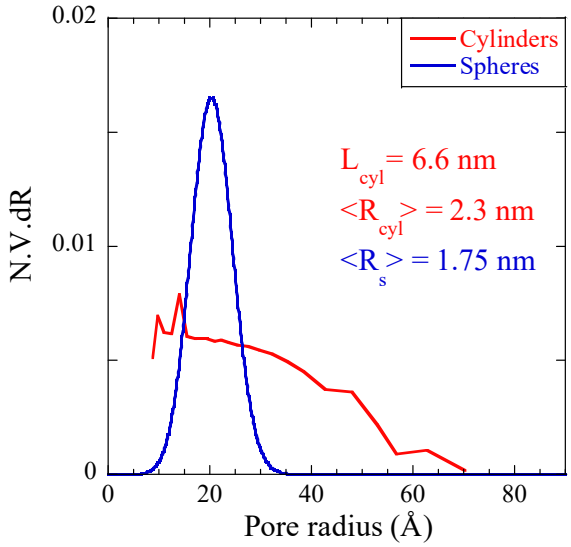
Cylinders
Spheres
L_cyl = 6.6 nm
<R_cyl> = 2.3 nm
<R_s> = 1.75 nm
N.V.dR
Pore radius (Å)

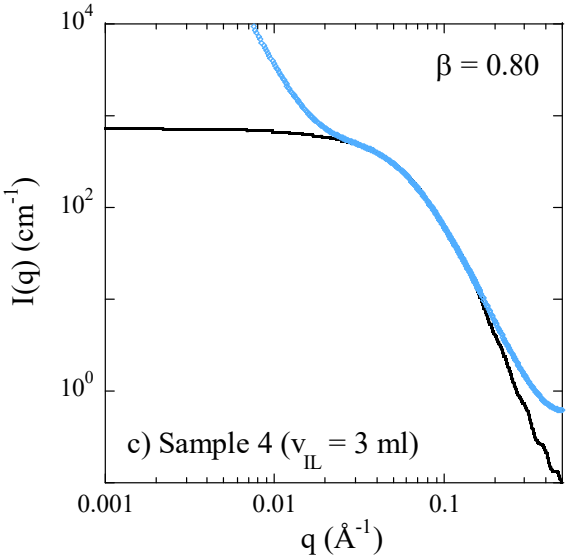
β = 0.80
c) Sample 4 (v_IL = 3 ml)
I(q) (cm^-1)
q (Å^-1)

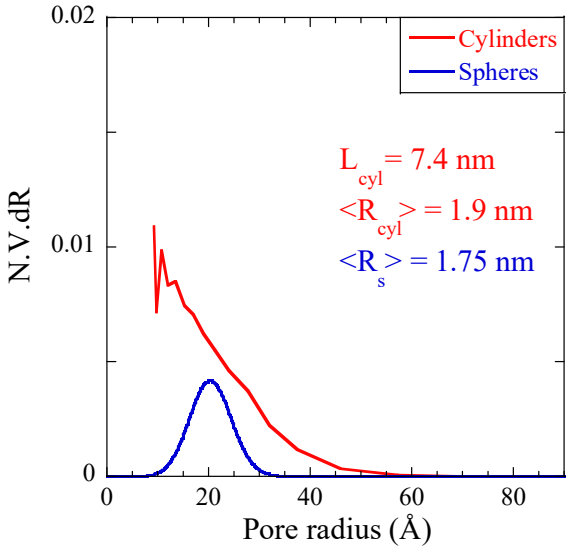
Cylinders
Spheres
L_cyl = 7.4 nm
<R_cyl> = 1.9 nm
<R_s> = 1.75 nm
N.V.dR
Pore radius (Å)

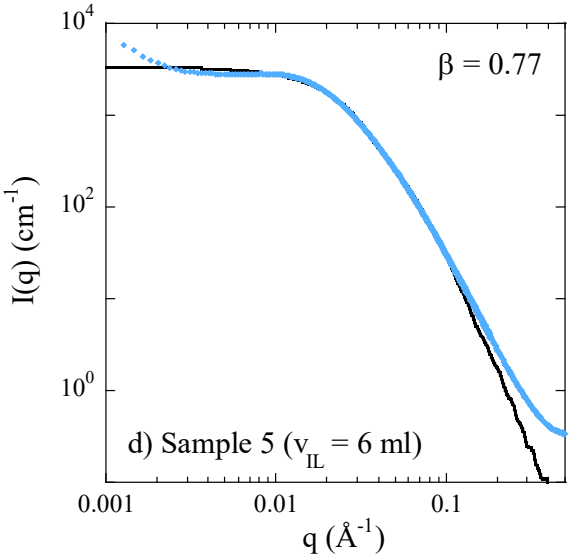
β = 0.77
d) Sample 5 (v_IL = 6 ml)
I(q) (cm^-1)
q (Å^-1)

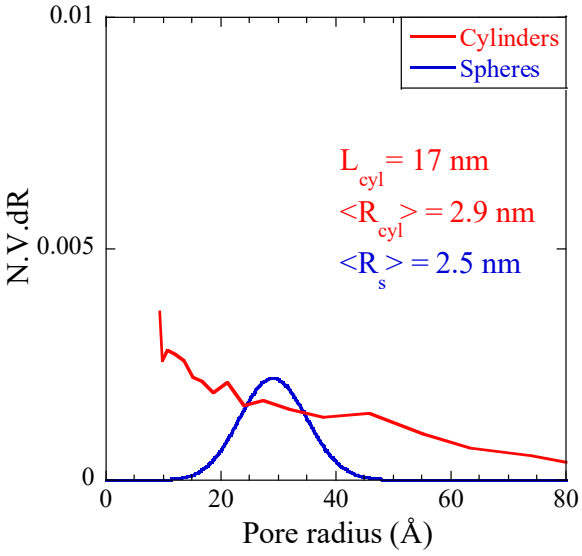
Cylinders
Spheres
L_cyl = 17 nm
<R_cyl> = 2.9 nm
<R_s> = 2.5 nm
N.V.dR
Pore radius (Å)

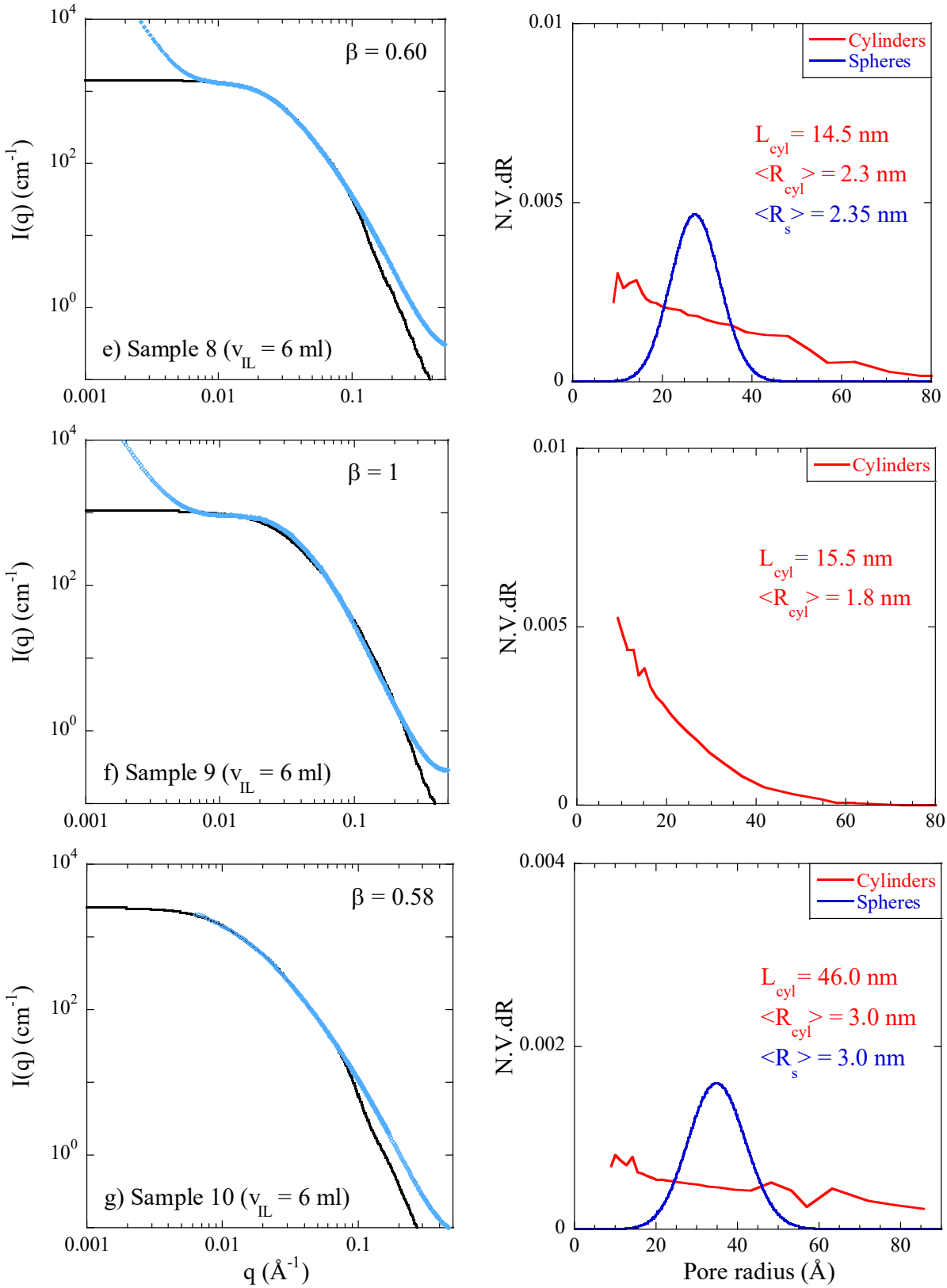

Figure S12: **Left part:** Fit (black solid line) of the scattered intensity of emptied film samples (symbols) by a superposition of cylinders of finite length and polydisperse in radius (from BJH) and polydisperse spheres. **Right part:** Corresponding pore size distributions of cylinders calculated using eq.(9) from BJH data, and of spheres, expressed as contribution to the total volume fraction. (a) Sample 1, correction of the prefactor = 1.10. (b) Sample 3, correction of the prefactor = 0.95. (c) Sample 4, correction of the prefactor = 1.40. (d) Sample 5, correction of the prefactor = 1.38. (e) Sample 8, correction of the prefactor = 1.06. (f) Sample 9, correction of the prefactor = 2.11. (g) Sample 10, correction of the prefactor = 0.80.

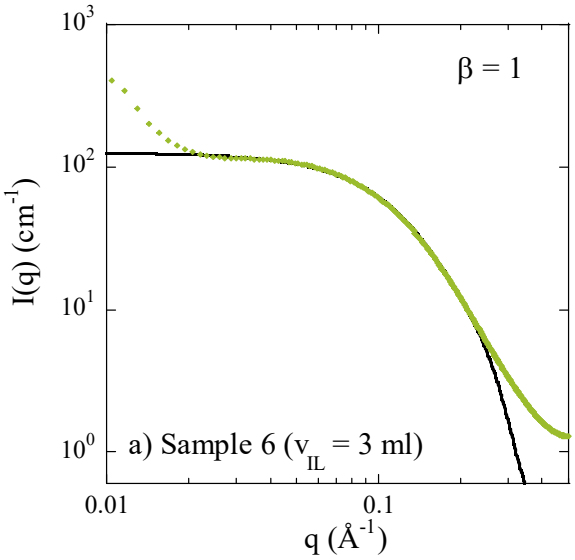
β = 1
a) Sample 6 (v_IL = 3 ml)
I(q) (cm^-1)
q (Å^-1)

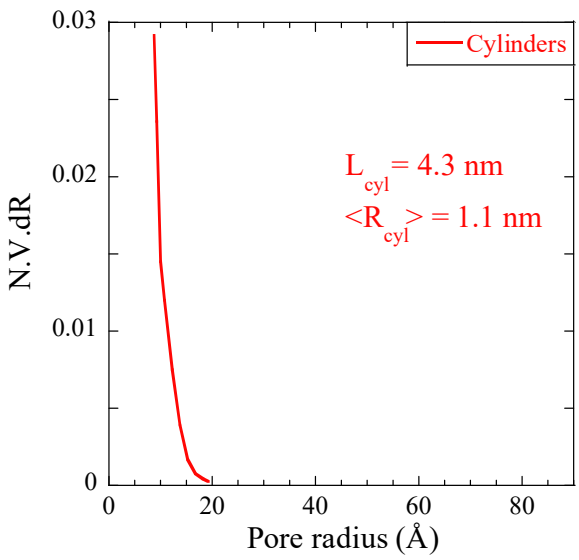
Cylinders
L_cyl = 4.3 nm
<R_cyl> = 1.1 nm
N.V.dR
Pore radius (Å)

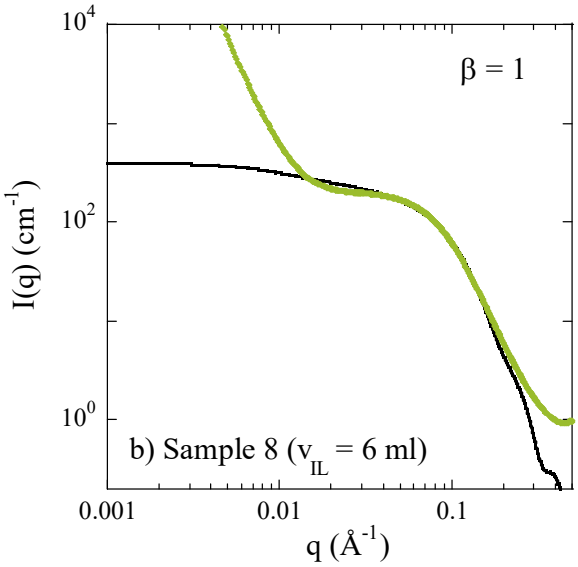
β = 1
b) Sample 8 (v_IL = 6 ml)
I(q) (cm^-1)
q (Å^-1)

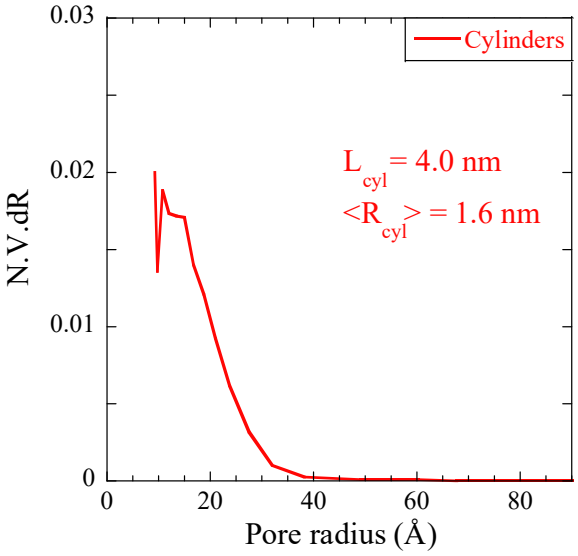
Cylinders
L_cyl = 4.0 nm
<R_cyl> = 1.6 nm
N.V.dR
Pore radius (Å)

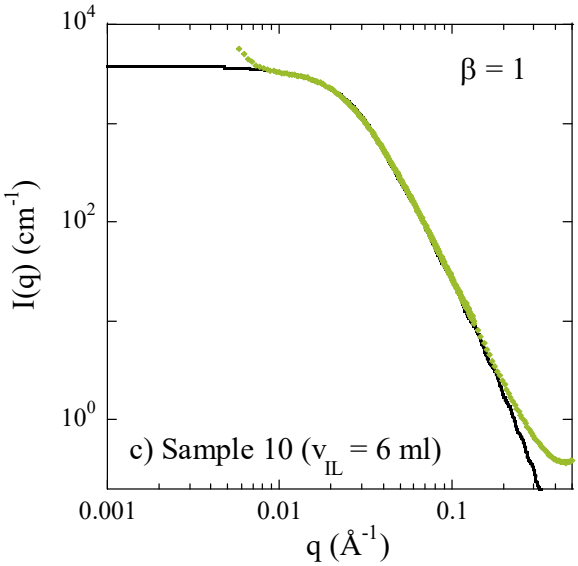
β = 1
c) Sample 10 (v_IL = 6 ml)
I(q) (cm^-1)
q (Å^-1)

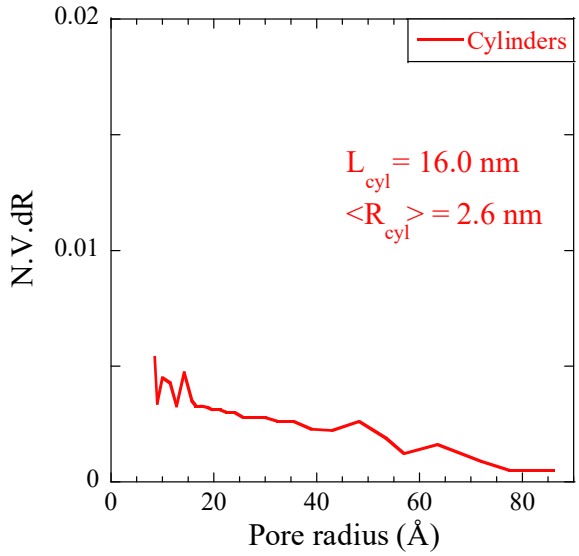
Cylinders
L_cyl = 16.0 nm
<R_cyl> = 2.6 nm
N.V.dR
Pore radius (Å)

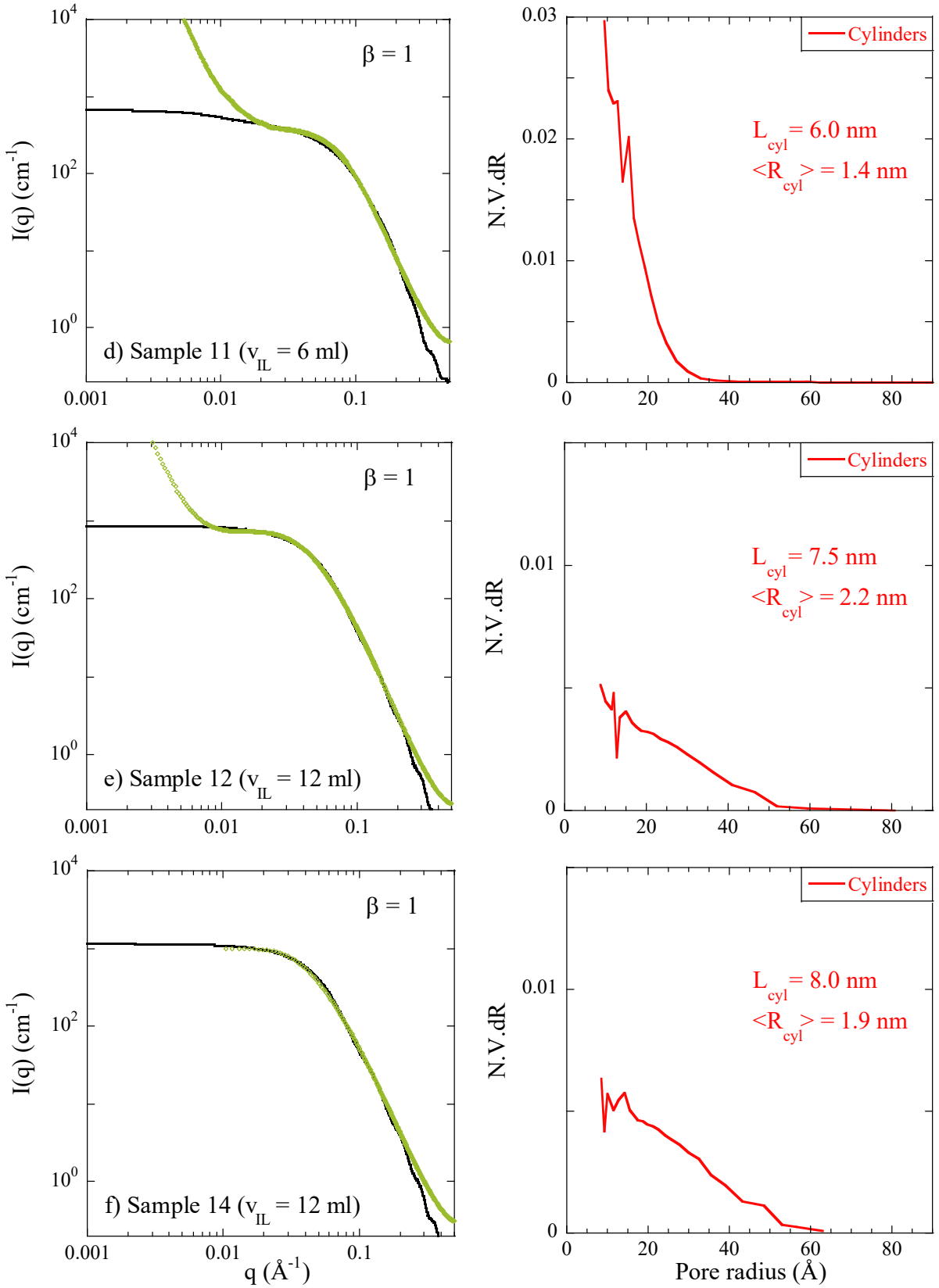

Figure S13: **Left part:** Fit (black solid line) of the scattered intensity of emptied monolith samples (symbols) by cylinders of finite length and polydisperse in radius (from BJH). **Right part:** Corresponding pore size distribution of cylinders calculated using eq.(9) from BJH data expressed as contribution to the total volume fraction. (a) Sample 6, correction of the prefactor = 4.63. (b) Sample 8, correction of the prefactor = 1.01. (c) Sample 10, correction of the prefactor = 1.17. (d) Sample 11, correction of the prefactor = 1.65. (e) Sample 12, correction of the prefactor = 2.17. (f) Sample 14, correction of the prefactor = 1.93.

The SAXS intensity of the monoliths with low IL incorporation (1 ml and 3 ml) are shown in Figure S14. In this case, the samples have no measurable mesoporosity by BET and the SAXS intensity is well described by short cylinders with a Gaussian distribution of radii. As observed in Figure S11, such a description is found to be better than considering spheres of the same polydispersity.

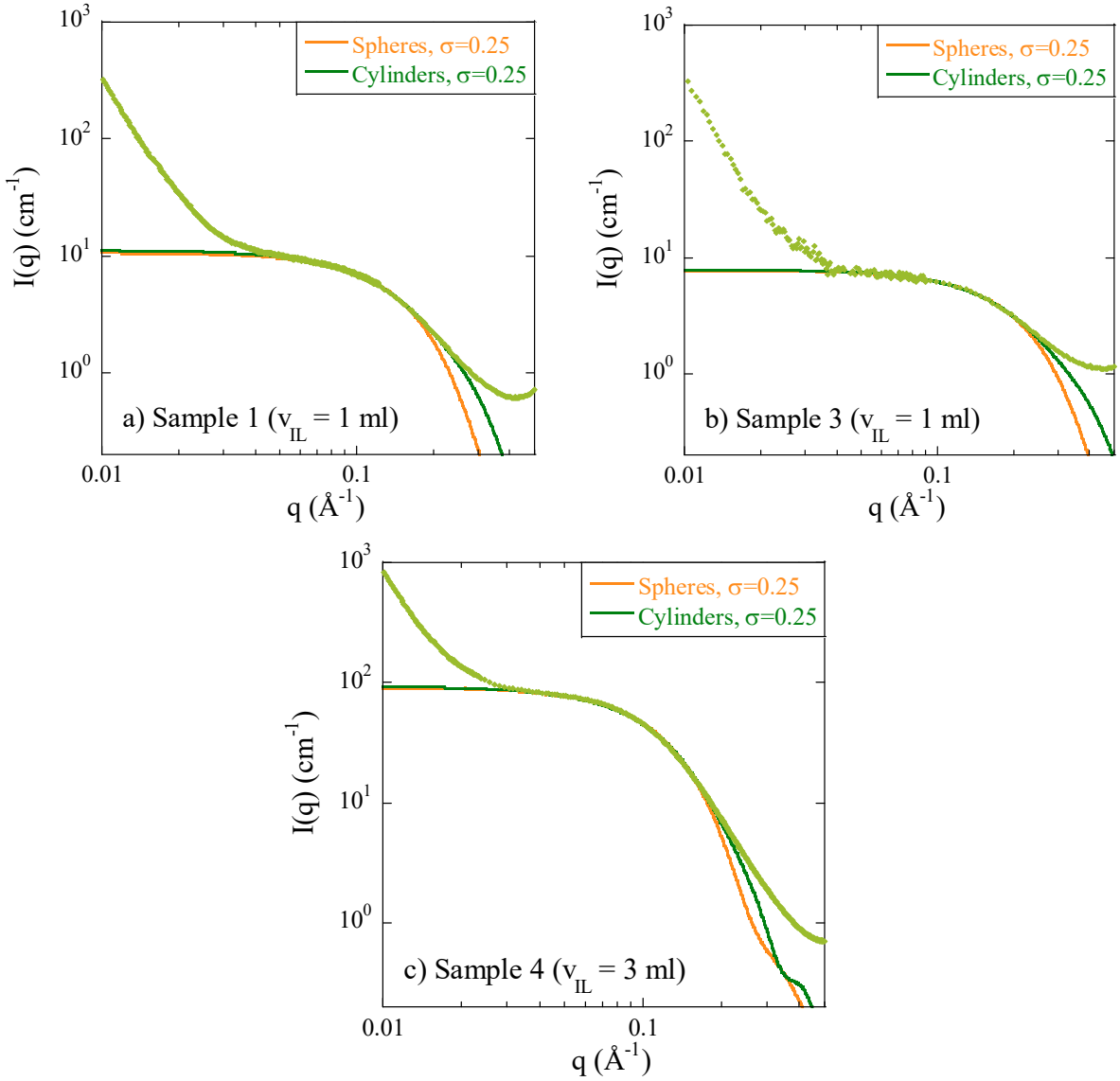

Figure S14. Fits of emptied monolith samples (see Table S2, green symbols) by polydisperse spheres (orange line) or radially polydisperse cylinders (green line), both using a Gaussian distribution with σ = 25%. (a) $\langle R_s \rangle$ = 1.1 nm for spheres, L_{cyl} = 3.6 nm and $\langle R_{cyl} \rangle$ = 0.7 nm for cylinders. (b) $\langle R_s \rangle$ = 0.81 nm for spheres, L_{cyl} = 2.6 nm and $\langle R_{cyl} \rangle$ = 0.5 nm for cylinders. (c) $\langle R_s \rangle$ = 1.4 nm for spheres, L_{cyl} = 4.0 nm and $\langle R_{cyl} \rangle$ = 1.05 nm for cylinders.

The volume fractions of cylinder ($\Phi_{cyl} = \beta\Phi_{meso}$) and sphere ($\Phi_s = (1-\beta)\Phi_{meso}$) in the SAXS description based on the BJH analysis are given in Figure S15, for both monoliths and films. For monoliths, there are only cylinders (β = 1 in all cases). This graph shows that the monoliths are located more in the middle, whereas the films extend also to the right indicating a higher IL incorporation. Also, the total volume fraction of mesopores is dominated by the cylinders and not by the small spheres. At high IL incorporation, both sphere and cylinder volume fractions tend to zero as the mesoporosity is reduced and replaced by macroporosity.

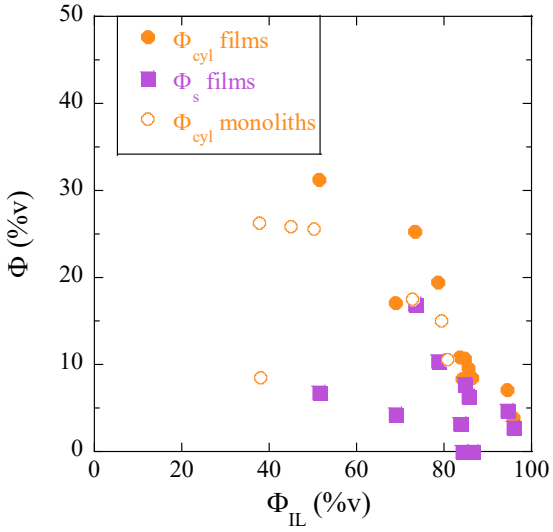

Figure S15. Summary plot of the mesopore volume fractions obtained from the SAXS analysis as a function of the total incorporated IL volume fraction. The solid symbols refer to films, and the empty ones to monoliths. Orange discs give the volume fraction of cylinders, and purple squares the volume fraction of spheres (only for films).